

Dynamics of the Kitaev-Heisenberg Model

Matthias Gohlke,¹ Ruben Verresen,^{1,2} Roderich Moessner,¹ and Frank Pollmann^{1,2}

¹Max-Planck-Institut für Physik komplexer Systeme, 01187 Dresden, Germany

²Department of Physics, T42, Technische Universität München, 85748 Garching, Germany

(Received 12 January 2017; revised manuscript received 29 May 2017; published 12 October 2017)

We introduce a matrix-product state based method to efficiently obtain dynamical response functions for two-dimensional microscopic Hamiltonians. We apply this method to different phases of the Kitaev-Heisenberg model and identify characteristic dynamical features. In the ordered phases proximate to the spin liquid, we find significant broad high-energy features beyond spin-wave theory, which resemble those of the Kitaev model. This establishes the concept of a proximate spin liquid, which was recently invoked in the context of inelastic neutron scattering experiments on α -RuCl₃. Our results provide an example of a natural path for proximate spin liquid features to arise at high energies above a conventionally ordered state, as the diffuse remnants of spin-wave bands intersect to yield a broad peak at the Brillouin zone center.

DOI: 10.1103/PhysRevLett.119.157203

Introduction.—The interplay of strong interactions and quantum fluctuations in spin systems can give rise to new and exciting physics. A prominent example is quantum spin liquids (QSLs), as fascinating as they are hard to detect: they lack local order parameters and are instead characterized in terms of emergent gauge fields. On the experimental side, spectroscopic measurements provide useful insights into such systems, particularly by probing the fractionalized excitations (e.g., deconfined spinons) accompanying the gauge field. Such measurements can be related to dynamical response functions, e.g., inelastic neutron scattering to the dynamical structure factor. On the theoretical side, determining the ground state properties of such quantum spin models is already a hard problem, and it is even more challenging to understand their dynamical properties.

Here, we present a combination of the density-matrix renormalization (DMRG) ground state method and a matrix-product state (MPS) based dynamical algorithm to obtain the response functions for generic two-dimensional spin systems. With this we are able to access the dynamics of exotic phases that can occur in frustrated systems. Moreover, it is also very useful for regular ordered phases where one would conventionally use large- S approximations, which in some cases cannot qualitatively explain certain high-energy features [1,2].

We demonstrate our method by applying it to the currently much-studied *Kitaev-Heisenberg model* (KHM) model on the honeycomb lattice,

$$H = \sum_{\langle i,j \rangle_\gamma} K_\gamma S_i^\gamma S_j^\gamma + J \sum_{\langle i,j \rangle} S_i \cdot S_j. \quad (1)$$

The first term is the pure Kitaev model exhibiting strongly anisotropic spin exchange coupling [3]. Neighboring spins couple depending on the direction of their bond γ with $S^x S^x$, $S^y S^y$, or $S^z S^z$ (Fig. 1). The second is the

$SU(2)$ -symmetric Heisenberg term. The KHM serves as a putative minimal model for several materials, including Na₂IrO₃, Li₂IrO₃ [4], and α -RuCl₃ [5]. The pure model is an exactly solvable spin-1/2 model stabilizing two different Kitaev quantum spin liquids (KSLs): a gapped \mathbb{Z}_2 one with Abelian excitations (the “A phase”) and one hosting gapless Majorana and gapped flux excitations (the “B phase”) [3]. If not stated otherwise, we use the parametrization $J = \cos \alpha$ and $K_\gamma = K = 2 \sin \alpha$. For $\alpha = \pm(\pi/2)$, we obtain the pure Kitaev model in the B phase, which is stable under time-reversal symmetric perturbations, as pointed out by Kitaev. Numerical studies of the ground state phase diagram of the KHM have shown an extended QSL phase for small J 's and four symmetry broken phases for larger J 's [4].

The dynamical response functions of the pure Kitaev model are known exactly and reveal characteristic features [6,7], such as a spectral gap in the dynamical spin structure factor due to a spin flip not only creating gapless Majorana but also gapped flux excitations. This feature is perturbatively stable to a small J [8], but the influence of J on high-energy features (or nonperturbatively at low energies) is

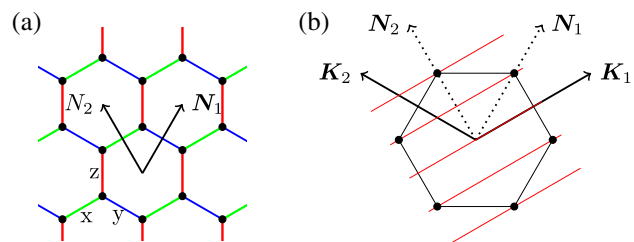


FIG. 1. (a) Green, red, and blue edges correspond to Kitaev exchange couplings $S_i^\gamma S_j^\gamma$ with $\gamma = x, y, z$. (b) Allowed \mathbf{k} vectors (the red lines) for an infinitely long cylinder with circumference $L_2 = 6$ and periodic boundary condition along N_2 . Black nodes picture the position of the gapless Majorana cones.

unclear and of ongoing interest [9]. More pressingly, there appear to be proximate spin liquids [10,11], such as, possibly, the currently much-studied α - RuCl_3 [2,5,11–19], whose low-energy physics is consistent with spin waves on an ordered background, but whose broad high-energy features resemble those of a KSL. Specifically, for intermediate energy scales, there are starlike features [2] apparently arising from a combination of spin-wave and QSL physics.

In this Letter, we first revisit the ground state phase diagram and confirm the previously found phases. The infinite cylinder geometry allows us to numerically confirm that the gaplessness of the KSL is robust throughout the entire phase. Second, we use a recently introduced MPS based time evolution algorithm [20] to obtain the dynamical spin structure factor. We benchmark our method by comparing it to exact results for the Kitaev model and find good agreement. We calculate the spectra of different (nonsoluble) phases of the KHM. Most notably, we identify broad high-energy continua even in ordered phases, which are, moreover, similar to the high-energy features in the nearby spin liquid phase. This provides a concrete realization of the concept of a proximate spin liquid, which was recently invoked in the context of neutron scattering experiments on α - RuCl_3 .

Ground state phase diagram.—We use the infinite size variant of the DMRG (iDMRG) algorithm on the KHM on infinite cylinders to map out the phase diagram. We choose cylinder geometries such that the corresponding momentum cuts contain the gapless Majorana modes of the Kitaev spin liquid. For the pure isotropic Kitaev model, there are gapless Majorana cones on the corners of the first Brillouin zone, Fig. 1(b). The full KHM has a C_6 symmetry, which means that in the 2D limit these cones cannot shift. The iDMRG method determines the ground state of systems of size $L_1 \times L_2$, where L_1 is in the thermodynamic limit and L_2 a finite circumference of up to 12 sites, being well beyond what is achievable in exact diagonalization. While, traditionally, iDMRG is used for finding the ground state of one-dimensional systems, it has become a fairly unbiased method for studying two-dimensional frustrated systems.

The resulting phase diagram for $L_2 = 12$ is shown in Fig. 2 (for the iDMRG simulations, we keep $\chi = 1200$ states), which agrees with previous studies [4,21–25]. For this L_2 , the system is compatible with the sublattice transformation that maps zigzag to antiferromagnetic (AFM) and stripy to ferromagnetic (FM) [22]. Plotted are the ground state energy and the entanglement or von Neumann entropy $S = -\text{Tr} \rho^{\text{red}} \log \rho^{\text{red}}$ of the reduced density matrix ρ^{red} for a bipartitioning of the cylinder by cutting along a ring. Both the cusps in the energy density and the discontinuities of the entanglement entropy indicate first order transitions. A careful finite size scaling is difficult because of the large bond dimension needed, and thus it is not possible to make definite statements about whether the transitions remain first order in the limit $L_2 \rightarrow \infty$. The symmetry broken phases can

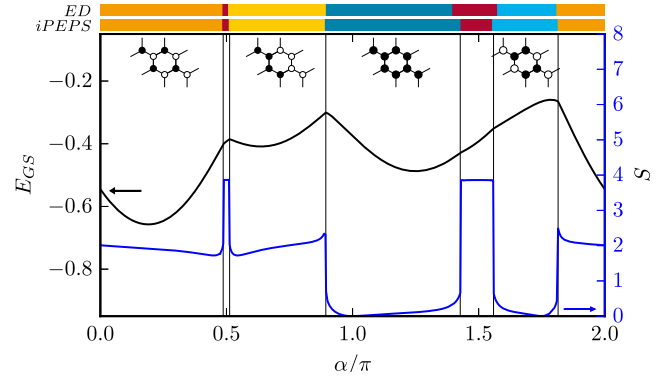


FIG. 2. Phase diagram for an infinite cylinder with circumference $L_2 = 12$ obtained using iDMRG. The black line corresponds to the ground state energy density, and the blue line to the entanglement entropy for a bipartition of the cylinder into a left and right half. (Insets) The ordering pattern of the magnetic phases. Two spin liquid phases exist around the pure Kitaev model ($\alpha = 0.5\pi$ and 1.5π). The results of exact diagonalization (ED) [4] and infinite PEPS [21] are illustrated at the top.

be identified by measuring the local magnetization. We identify a Néel phase ($-0.185 < \alpha/\pi < 0.487$) that extends around the pure antiferromagnetic Heisenberg [26] point, the corresponding zigzag phase ($0.513 < \alpha/\pi < 0.894$), a ferromagnetic phase around the pure FM Heisenberg point ($0.894 < \alpha/\pi < 1.427$), and its stripy phase ($1.559 < \alpha/\pi < 1.815$). The two KSLs between Néel and zigzag as well as between FM and stripy are confirmed to be gapless, as expected for the B phase. For example, if L_2 is a multiple of 6, we use the finite-entanglement scaling approach [29–31] and extract the expected chiral central charge $c = 1$ for both KSLs [28], with each of the two Majorana cones contributing $c = 1/2$. Note that when a gapless spin liquid is placed on a cylinder, the gauge field generically adjusts to open a gap [34]. In order to see gapless behavior, we have to initiate the iDMRG simulations in the gapless sector to access a metastable state [28]. The gapped ground state having a nonzero flux through the cylinder overestimates the stability of the QSL phases. It is notable how well the phase boundaries agree with those from the infinite projected entangled pair state (iPEPS) simulations [21].

Dynamical spin structure factor $S(\mathbf{k}, \omega)$.—Starting from a ground state obtained using iDMRG, we calculate $S(\mathbf{k}, \omega)$ by Fourier transforming the dynamical correlation function $C^{\gamma\gamma}(\mathbf{r}, t) = \langle S_r^\gamma(t) S_0^\gamma(0) \rangle$. The real-time correlations can be efficiently obtained using a recently introduced matrix-product operator based time evolution method [20]. This allows for long-range interactions resulting from unraveling the cylinder to a one-dimensional system which render standard methods like the time-evolving block decimation inefficient. Following the general strategy laid out in Refs. [35–37], we perform the simulations for an infinite cylinder with a fixed circumference. Note that the entanglement growth and the resulting growth of the

required number of states is generically slow, as the ground state is only locally perturbed, and thus long times can be reached even in the cylinder geometry. We show results obtained for $0 \leq t \leq T$ and, to avoid Gibbs oscillations, we multiply our real-time data by a Gaussian ($\sigma_t \approx 0.43T$). This corresponds to a broadening in ω space ($\sigma_\omega \approx (2.3/T)$). We use linear prediction to allow room for the tail of the Gaussian in real time, but we confirm that the final results do not depend on its details [38]. Thence,

$$\mathcal{S}^{\gamma\gamma}(\mathbf{k}, \omega) = \frac{1}{2\pi} \sum_{\mathbf{r}} \int_{-\infty}^{\infty} e^{i(\omega t - \mathbf{k} \cdot \mathbf{r})} C^{\gamma\gamma}(\mathbf{r}, t) dt,$$

which is normalized as $\int \mathcal{S}^{\gamma\gamma}(\mathbf{k}, \omega) d\mathbf{k} d\omega = \int d\mathbf{k}$. Unless stated otherwise, we present results for $\mathcal{S}(\mathbf{k}, \omega) = \sum_{\gamma} \mathcal{S}^{\gamma\gamma}(\mathbf{k}, \omega)$.

We benchmark the method by comparing our numerical approach to exact results for the pure Kitaev model. Figure 3(a) shows a comparison for the gapped Kitaev model in the A phase with $K_x/K_{y,z} = 6$, with the exact solution for $\mathcal{S}^{zz}(\mathbf{k} = 0, \omega)$ shown in black. Our numerics (with resolution $\sigma_\omega \approx 0.06$ in the units shown) for an infinite cylinder with $L_2 = 10$ (red) agrees well with such features as gap, bandwidth, and total spectral weight. In the real-time data (inset), while the numerics agrees with the exact solution for the cylinder geometry, it overlaps with the 2D result only until a characteristic time scale corresponding to the perturbation traveling around the cylinder and then feeling the static fluxes inserted by the spin flip. More generally, we expect such time scales (after which 2D physics becomes 1D) to be particularly significant for systems with fractionalization. For Fig. 3(b), we take $K_x = K_y = K_z = -2$ to be in the gapless KSL phase, the B phase, at $\alpha = (3\pi/2)$. Comparing the exact 2D result (black) to our numerics for a cylinder of circumference $L_2 = 6$ (red), we see qualitative similarities, such as a spectral gap (the dashed lines; slightly obscured by our finite-time window), a dip where the fluxes suppress the van Hove singularity of the Majorana spectrum [6], comparable bandwidth, and strong low-energy weight. To better resolve the spectral gap, we rely slightly on linear prediction [38] by using a real-time Gaussian envelope with $\sigma_t = 0.56T$, corresponding to $\sigma_\omega \approx 0.045$. Two striking quantitative differences are (i) the spectral gap which for this circumference is approximately half that of the 2D limit, and (ii) the presence of a delta peak on this gap ($\approx 4\%$ of total spectral weight). The latter, present for any cylinder, vanishes as $L_2 \rightarrow \infty$ [39]. The inset compares exact real-time results for the cylinder [40] with our numerics. Despite approximating the ground state of the gapless sector using MPS, we find good agreement for appreciable times.

After this benchmarking, we explore $\mathcal{S}(\mathbf{k}, \omega)$ in different phases of the KHM shown in Fig. 4, all with $\sigma_\omega \approx 0.06$. The pure Heisenberg FM ($\alpha = \pi$) can be solved in terms of

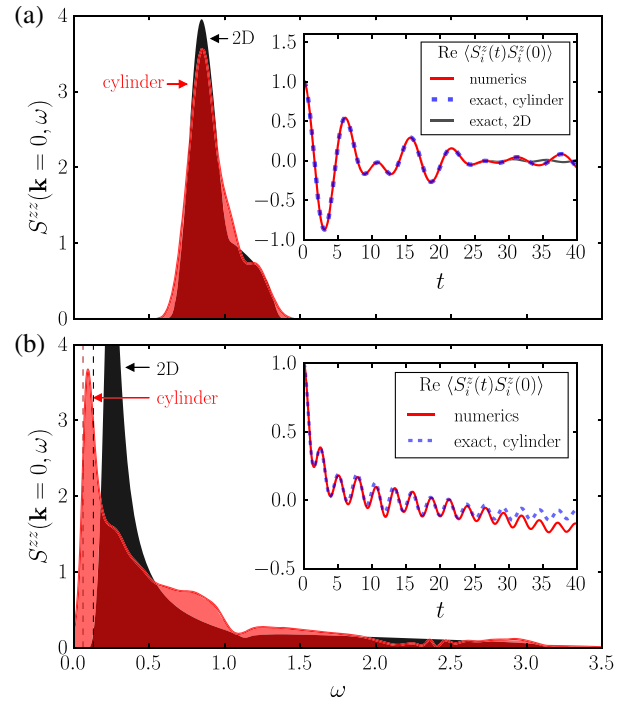


FIG. 3. Dynamical spin structure factor $\mathcal{S}^{zz}(\mathbf{k} = 0, \omega)$ from our numerical approach compared with the exact result (the insets show real-time data). Exact results were obtained following Ref. [6], except for the blue curve in (b) [40]. (a) Gapped KSL, A phase, on a cylinder with $L_2 = 10$ and anisotropic couplings $K_x = -2$ and $K_y = K_z = -(1/3)$. (b) Gapless isotropic KSL, B phase, with $L_2 = 6$ and $\alpha = (3\pi/2)$.

linear spin-wave theory (LSWT) and numerically captured with bond dimension $\chi = 2$. Instead of this special point, in Fig. 4(a) we show results for $\alpha = 1.1\pi$ (corresponding to $K = 0.65J$), where we still find excellent agreement with LSWT. Note that there is a small gap ($\approx 0.05|J|$) which is absent in LSWT despite the presence of $SU(2)$ -breaking Kitaev coupling [4]. We do not observe any strong cylinder effects on the dynamics, which is presumably related to the short correlation length and the absence of fractional excitations. The pure Heisenberg AFM (with small XXZ anisotropy) in Fig. 4(b) shows appreciable deviations from LSWT, with second order SWT [41] giving better agreement. Moreover, the weight in the spin waves is approximately halved, indicating the importance of higher order magnon contributions. Staying within the Néel phase but approaching the QSL, LSWT cannot even qualitatively describe Fig. 4(c), with much weight in very broad high-energy features unaccounted for.

Lastly, we focus on a parameter regime producing zigzag ordering like that found in $\alpha\text{-RuCl}_3$ [2,11,12]. Figure 5 shows $\mathcal{S}(\mathbf{k}, \omega)$ for four different choices of α : the first row contains the exact solution for the pure AFM Kitaev model, and the subsequent rows are all numerical results within the zigzag phase with increasing α . For each α , we show $\mathcal{S}(\mathbf{k}, \omega)$ at a fixed ω : the columns display representative

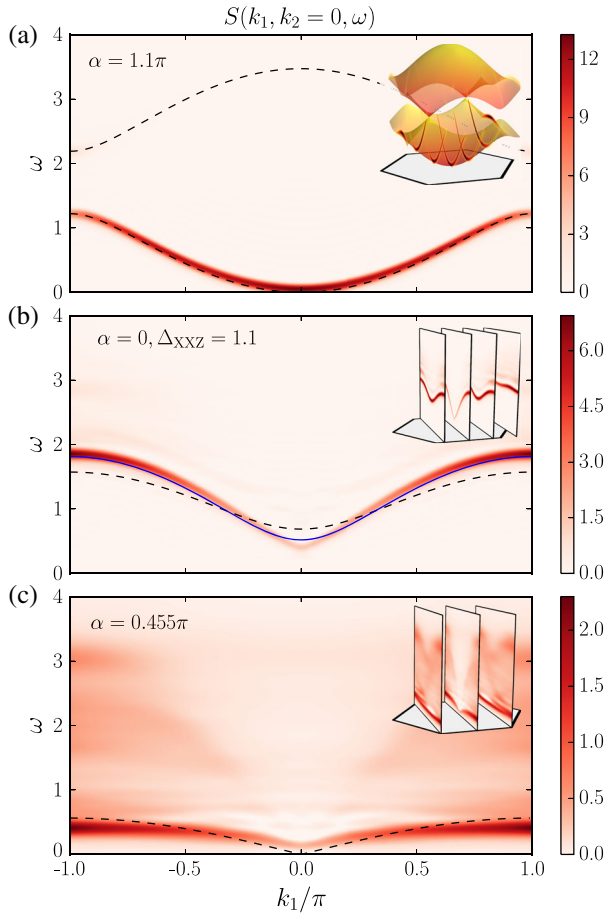


FIG. 4. $S(\mathbf{k}, \omega)$ for cuts $\mathbf{k} = (k_x, 0)$ in different phases of the KHM with an ω resolution $\sigma_\omega \approx 0.06$. Dashed lines show the results from LSWT. (Insets) The data for all allowed cuts. (a) FM phase for a cylinder with $L_2 = 12$. (b) Antiferromagnet with small spin anisotropy without a Kitaev term ($L_2 = 8$). The solid blue line shows next order spin-wave calculations [41]. (c) AFM phase in proximity to the KSL ($L_2 = 6$).

low-, mid-, and high-energy features, with parameters $L_2 = 12$ and time cutoff $T = 10$ corresponding to $\sigma_\omega \approx 0.23$. We average over the different symmetry broken directions. Results for $L_2 = 6$ and $T = 40$ reveal that, even at this resolution, the high-energy features stay very broad [28]. The first column shows the low-energy physics of the Kitaev model being reconstructed into spin-wave bands, with minima on the edges of the first Brillouin zone. For $\alpha = 0.7\pi$ and 0.8π , these obey the C_6 symmetry, indicating that the cylinder geometry locally looks to be 2D. Interestingly, the high-energy physics of the ordered phases is very similar to that of the pure Kitaev model: broad features are centered around the symmetric Γ point, $\mathbf{k} = 0$, with its characteristic energy and width simultaneously decreasing as α increases. The interplay between these low- and high-energy features then gives rise to different midenergy shapes. In fact, the six spin-wave bands start on the edges of the first Brillouin zone. As the energy

increases, these bands become increasingly diffuse, eventually overlapping in a very broad blob at Γ . Both the spin waves and the blob sharpen as one moves away from the nearby QSL. The persistence of the broad high-energy features characteristic of the QSL across the transition into the zigzag phase are the essence of the idea of a proximate spin liquid. This concept was recently invoked for the putative Kitaev compound α - RuCl_3 [2,4,5,11]. However, its detailed microscopic Hamiltonian, while not yet universally agreed upon, likely contains important terms beyond the KHM studied here [13,42–44]. Note that in Fig. 5, for $\alpha = 0.7\pi$ at intermediate energies, there is a six-pointed star whose arms point towards the edges of the first Brillouin zone. It is interesting to note that if we do not average over different symmetry broken directions, the low-energy physics strongly breaks the C_6 symmetry, yet the six-pointed star at intermediate energies persists; thus, even if we interpret these high-energy features as the overlap of broad spin waves, at this point, the effect of symmetry breaking has disappeared. Under what conditions such a symmetry restoration occurs more generally is an interesting question, as is the issue regarding which

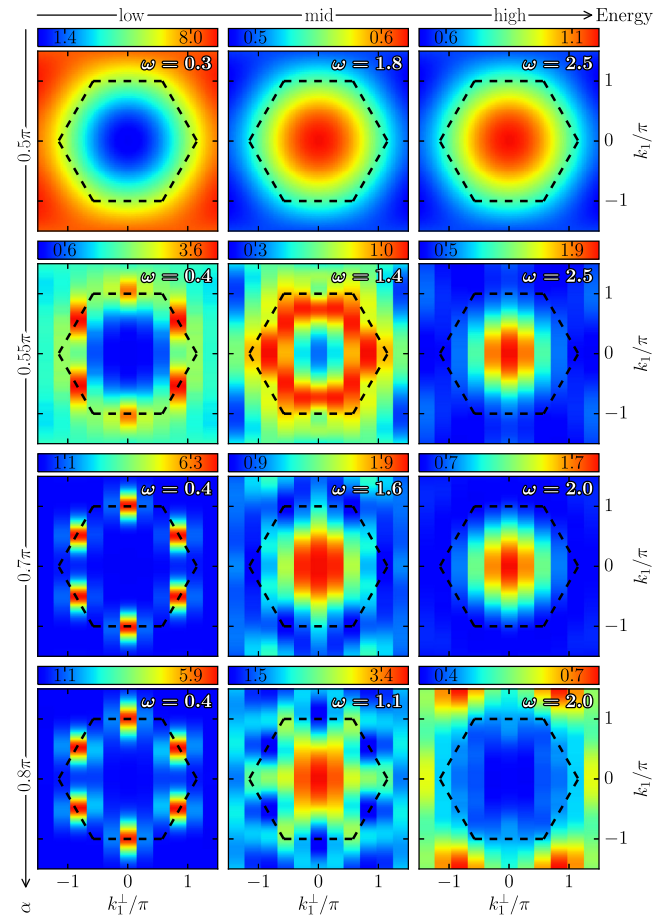


FIG. 5. $S(\mathbf{k}, \omega)$ at three different energies for four models: KSL at $\alpha = 0.5\pi$ (analytic result, 2D) and zigzag order at $\alpha = 0.55\pi$, 0.7π , and 0.8π (with $L_2 = 12$).

settings a broad response at intermediate and high energies may generally be expected to occur, and to what extent it may nonetheless be amenable to a quasiparticle description.

Conclusion.—We have presented a new method for obtaining the dynamical properties of generic lattice spin models in (quasi) two dimensions, which we expect to be useful for many future studies. In the KHM, our study reveals several features beyond spin-wave theory even in the ordered phases, providing a concrete realization of the concept of a proximate spin liquid.

We are grateful to Roser Valenti, Mike Zaletel, and Johannes Knolle for the stimulating discussions. We thank Johannes in particular for providing unpublished data for the dynamical correlations of the isotropic Kitaev model on the cylinder. This work was supported in part by Deutsche Forschungsgemeinschaft via SFB 1143 and Research Unit FOR 1807 through Grant No. PO 1370/2-1.

M. G. and R. V. contributed equally to this work.

-
- [1] B. Dalla Piazza, M. Mourigal, N. B. Christensen, G. J. Nilsen, P. Tregenna-Piggott, T. G. Perring, M. Enderle, D. F. McMorrow, D. A. Ivanov, and H. M. Rønnow, *Nat. Phys.* **11**, 62 (2015).
- [2] A. Banerjee, J. Yan, J. Knolle, C. A. Bridges, M. B. Stone, M. D. Lumsden, D. G. Mandrus, D. A. Tennant, R. Moessner, and S. E. Nagler, *Science* **356**, 1055 (2017).
- [3] A. Kitaev, *Ann. Phys. (Amsterdam)* **321**, 2 (2006).
- [4] J. Chaloupka, G. Jackeli, and G. Khaliullin, *Phys. Rev. Lett.* **110**, 097204 (2013).
- [5] K. W. Plumb, J. P. Clancy, L. J. Sandilands, V. V. Shankar, Y. F. Hu, K. S. Burch, H.-Y. Kee, and Y.-J. Kim, *Phys. Rev. B* **90**, 041112 (2014).
- [6] J. Knolle, D. L. Kovrizhin, J. T. Chalker, and R. Moessner, *Phys. Rev. Lett.* **112**, 207203 (2014).
- [7] J. Knolle, G.-W. Chern, D. L. Kovrizhin, R. Moessner, and N. B. Perkins, *Phys. Rev. Lett.* **113**, 187201 (2014).
- [8] X.-Y. Song, Y.-Z. You, and L. Balents, *Phys. Rev. Lett.* **117**, 037209 (2016).
- [9] D. Gotfryd, J. Rusnačko, K. Wohlfeld, G. Jackeli, J. Chaloupka, and A. M. Oleś, *Phys. Rev. B* **95**, 024426 (2017).
- [10] T. Suzuki, T. Yamada, Y. Yamaji, and S.-i. Suga, *Phys. Rev. B* **92**, 184411 (2015).
- [11] A. Banerjee, C. A. Bridges, J.-Q. Yan, A. A. Aczel, L. Li, M. B. Stone, G. E. Granroth, M. D. Lumsden, Y. Yiu, J. Knolle, S. Bhattacharjee, D. L. Kovrizhin, R. Moessner, D. A. Tennant, D. G. Mandrus, and S. E. Nagler, *Nat. Mater.* **15**, 733 (2016).
- [12] R. D. Johnson, S. C. Williams, A. A. Haghighirad, J. Singleton, V. Zapf, P. Manuel, I. I. Mazin, Y. Li, H. O. Jeschke, R. Valenti, and R. Coldea, *Phys. Rev. B* **92**, 235119 (2015).
- [13] H.-S. Kim and H.-Y. Kee, *Phys. Rev. B* **93**, 155143 (2016).
- [14] L. J. Sandilands, Y. Tian, A. A. Reijnders, H.-S. Kim, K. W. Plumb, Y.-J. Kim, H.-Y. Kee, and K. S. Burch, *Phys. Rev. B* **93**, 075144 (2016).
- [15] L. J. Sandilands, C. H. Sohn, H. J. Park, S. Y. Kim, K. W. Kim, J. A. Sears, Y.-J. Kim, and T. W. Noh, *Phys. Rev. B* **94**, 195156 (2016).
- [16] J. Chaloupka and G. Khaliullin, *Phys. Rev. B* **94**, 064435 (2016).
- [17] F. Lang, P. J. Baker, A. A. Haghighirad, Y. Li, D. Prabhakaran, R. Valenti, and S. J. Blundell, *Phys. Rev. B* **94**, 020407 (2016).
- [18] G. B. Halász, N. B. Perkins, and J. van den Brink, *Phys. Rev. Lett.* **117**, 127203 (2016).
- [19] A. Koitzsch, C. Habenicht, E. Müller, M. Knupfer, B. Büchner, H. C. Kandpal, J. van den Brink, D. Nowak, A. Isaeva, and T. Doert, *Phys. Rev. Lett.* **117**, 126403 (2016).
- [20] M. P. Zaletel, R. S. K. Mong, C. Karrasch, J. E. Moore, and F. Pollmann, *Phys. Rev. B* **91**, 165112 (2015).
- [21] J. Osorio Iregui, P. Corboz, and M. Troyer, *Phys. Rev. B* **90**, 195102 (2014).
- [22] J. Chaloupka, G. Jackeli, and G. Khaliullin, *Phys. Rev. Lett.* **105**, 027204 (2010).
- [23] H.-C. Jiang, Z.-C. Gu, X.-L. Qi, and S. Trebst, *Phys. Rev. B* **83**, 245104 (2011).
- [24] E. Sela, H.-C. Jiang, M. H. Gerlach, and S. Trebst, *Phys. Rev. B* **90**, 035113 (2014).
- [25] K. Shinjo, S. Sota, and T. Tohyama, *Phys. Rev. B* **91**, 054401 (2015).
- [26] Note that, due to the mapping of the 2D lattice onto a 1D chain, the Mermin-Wagner-Coleman theorem [27] applies at the pure AFM Heisenberg point and suppresses long-range Néel order. In fact, it is replaced by a gapped symmetry-preserving state, which extends over a finite region in parameter space. For further discussion, see the Supplemental Material [28].
- [27] S. Coleman, *Commun. Math. Phys.* **31**, 259 (1973).
- [28] See Supplemental Material at <http://link.aps.org/supplemental/10.1103/PhysRevLett.119.157203>, which includes Refs. [9,21,27,29–33], for further discussion of 1D vs 2D for the Heisenberg AFM, KSL sectors on a cylinder, finite-entanglement scaling, and $L_2 = 6$ dynamics.
- [29] P. Calabrese and J. Cardy, *J. Stat. Mech.* (2004) P06002.
- [30] L. Tagliacozzo, T. R. de Oliveira, S. Iblisdir, and J. I. Latorre, *Phys. Rev. B* **78**, 024410 (2008).
- [31] F. Pollmann, S. Mukerjee, A. M. Turner, and J. E. Moore, *Phys. Rev. Lett.* **102**, 255701 (2009).
- [32] J. D. Reger, J. A. Riera, and A. P. Young, *J. Phys. Condens. Matter* **1**, 1855 (1989).
- [33] S. R. White, R. M. Noack, and D. J. Scalapino, *Phys. Rev. Lett.* **73**, 886 (1994).
- [34] Y.-C. He, M. P. Zaletel, M. Oshikawa, and F. Pollmann, *Phys. Rev. X* **7**, 031020 (2017).
- [35] J. A. Kjäll, F. Pollmann, and J. E. Moore, *Phys. Rev. B* **83**, 020407 (2011).
- [36] H. N. Phien, G. Vidal, and I. P. McCulloch, *Phys. Rev. B* **86**, 245107 (2012).
- [37] V. Zauner, M. Ganahl, H. G. Evertz, and T. Nishino, *J. Phys. Condens. Matter* **27**, 425602 (2015).
- [38] S. R. White and I. Affleck, *Phys. Rev. B* **77**, 134437 (2008).
- [39] We used free-fermion exact diagonalization (which allows for system sizes of thousands of sites) to extract the weight

of this peak for $L_2 = 6$ and confirmed that it vanishes as $L_2 \rightarrow \infty$, which is consistent with analytic results in the 2D limit [6].

[40] J. Knolle (unpublished).

[41] Z. Weihong, J. Oitmaa, and C. J. Hamer, *Phys. Rev. B* **44**, 11869 (1991).

[42] R. Yadav, N. A. Bogdanov, V. M. Katukuri, S. Nishimoto, J. van den Brink, and L. Hozoi, *Sci. Rep.* **6**, 37925 (2016).

[43] W. Wang, Z.-Y. Dong, S.-L. Yu, and J.-X. Li, *Phys. Rev. B* **96**, 115103 (2017).

[44] S. M. Winter, K. Riedl, A. Honecker, and R. Valenti, [arXiv:1702.08466](https://arxiv.org/abs/1702.08466).